

This is a repository copy of *First measurement of polarisation transfer  $C^n_{\{x\}}$  in deuteron photodisintegration and the signatures of the  $d^{*(2380)}$  hexaquark.*

White Rose Research Online URL for this paper:

<https://eprints.whiterose.ac.uk/200248/>

---

**Preprint:**

(2022) First measurement of polarisation transfer  $C^n_{\{x\}}$  in deuteron photodisintegration and the signatures of the  $d^{*(2380)}$  hexaquark. [Preprint]

---

**Reuse**

Items deposited in White Rose Research Online are protected by copyright, with all rights reserved unless indicated otherwise. They may be downloaded and/or printed for private study, or other acts as permitted by national copyright laws. The publisher or other rights holders may allow further reproduction and re-use of the full text version. This is indicated by the licence information on the White Rose Research Online record for the item.

**Takedown**

If you consider content in White Rose Research Online to be in breach of UK law, please notify us by emailing [eprints@whiterose.ac.uk](mailto:eprints@whiterose.ac.uk) including the URL of the record and the reason for the withdrawal request.

# First measurement of polarisation transfer $C_{x'}^n$ in deuteron photodisintegration and the signatures of the $d^*(2380)$ hexaquark.

M. Bashkanov<sup>a</sup>, D.P. Watts<sup>a</sup>, S. Kay<sup>b</sup>, S. Abt<sup>e</sup>, P. Achenbach<sup>f</sup>, P. Adlarson<sup>f</sup>, F. Afzal<sup>g</sup>, Z. Ahmed<sup>b</sup>, C.S. Akondi<sup>c</sup>, J.R.M. Annand<sup>d</sup>, H.J. Arends<sup>f</sup>, R. Beck<sup>g</sup>, M. Biroth<sup>f</sup>, N. Borisov<sup>h</sup>, A. Braghieri<sup>i</sup>, W.J. Briscoe<sup>j</sup>, F. Cividini<sup>f</sup>, C. Collicott<sup>k</sup>, S. Costanza<sup>li</sup>, A. Denig<sup>f</sup>, E.J. Downie<sup>j</sup>, P. Drexler<sup>m,f</sup>, S. Fegan<sup>a</sup>, A. Fix<sup>v</sup>, S. Gardner<sup>d</sup>, D. Ghosal<sup>e</sup>, D.I. Glazier<sup>d</sup>, I. Gorodnov<sup>h</sup>, W. Gradl<sup>f</sup>, M. Günther<sup>e</sup>, D. Gurevich<sup>n</sup>, L. Heijmanskjöld<sup>f</sup>, D. Hornidge<sup>o</sup>, G.M. Huber<sup>b</sup>, A. Käser<sup>e</sup>, V.L. Kashevarov<sup>f,h</sup>, M. Korolija<sup>p</sup>, B. Krusche<sup>e</sup>, A. Lazarev<sup>h</sup>, K. Livingston<sup>d</sup>, S. Lutterer<sup>e</sup>, I.J.D. MacGregor<sup>d</sup>, D.M. Manley<sup>c</sup>, P.P. Martel<sup>f,o</sup>, R. Miskimen<sup>q</sup>, E. Mornacchi<sup>f</sup>, C. Mullen<sup>d</sup>, A. Neganov<sup>h</sup>, A. Neiser<sup>f</sup>, M. Ostrick<sup>f</sup>, P.B. Otte<sup>f</sup>, D. Paudyal<sup>b</sup>, P. Pedroni<sup>i</sup>, A. Powell<sup>d</sup>, S.N. Prakhov<sup>r</sup>, V. Sokhoyan<sup>f</sup>, K. Spieker<sup>g</sup>, O. Steffen<sup>f</sup>, I.I. Strakovsky<sup>j</sup>, T. Strub<sup>e</sup>, I. Supek<sup>p</sup>, A. Thiel<sup>g</sup>, M. Thiel<sup>f</sup>, A. Thomas<sup>f</sup>, Yu.A. Usov<sup>h</sup>, S. Wagner<sup>f</sup>, J. Wettig<sup>f</sup>, M. Wolfes<sup>f</sup>, N. Zachariou<sup>a</sup>

<sup>a</sup>Department of Physics, University of York, Heslington, York, YO10 5DD, UK

<sup>b</sup>University of Regina, Regina, SK S4S-0A2 Canada

<sup>c</sup>Kent State University, Kent, Ohio 44242, USA

<sup>d</sup>SUPA School of Physics and Astronomy, University of Glasgow, Glasgow, G12 8QQ, UK

<sup>e</sup>Department of Physics, University of Basel, CH-4056 Basel, Switzerland

<sup>f</sup>Institut für Kernphysik, University of Mainz, D-55099 Mainz, Germany

<sup>g</sup>Helmholtz-Institut für Strahlen- und Kernphysik, University Bonn, D-53115 Bonn, Germany

<sup>h</sup>Joint Institute for Nuclear Research, 141980 Dubna, Russia

<sup>i</sup>INFN Sezione di Pavia, I-27100 Pavia, Pavia, Italy

<sup>j</sup>Center for Nuclear Studies, The George Washington University, Washington, DC 20052, USA

<sup>k</sup>Department of Astronomy and Physics, Saint Mary's University, E4L1E6 Halifax, Canada

<sup>l</sup>Dipartimento di Fisica, Università di Pavia, I-27100 Pavia, Italy

<sup>m</sup>II. Physikalisches Institut, University of Giessen, D-35392 Giessen, Germany

<sup>n</sup>Institute for Nuclear Research, RU-125047 Moscow, Russia

<sup>o</sup>Mount Allison University, Sackville, New Brunswick E4L1E6, Canada

<sup>p</sup>Rudjer Boskovic Institute, HR-10000 Zagreb, Croatia

<sup>q</sup>University of Massachusetts, Amherst, Massachusetts 01003, USA

<sup>r</sup>University of California Los Angeles, Los Angeles, California 90095-1547, USA

<sup>s</sup>Racah Institute of Physics, Hebrew University of Jerusalem, Jerusalem 91904, Israel

<sup>t</sup>Department of Physics and Astronomy, Rutgers University, Piscataway, New Jersey, 08854-8019

<sup>u</sup>Jefferson Lab, 12000 Jefferson Ave., Newport News, VA 23606, USA

<sup>v</sup>Tomsk Polytechnic University, 634034 Tomsk, Russia

arXiv:2206.12299v2 [nucl-ex] 29 Sep 2022

## Abstract

A first measurement of the polarisation transfer from a circularly-polarised photon to the final state neutron ( $C_{x'}^n$ ) in deuteron photodisintegration has been carried out. This quantity is determined over the photon energy range 370 – 700 MeV and for neutron centre-of-mass breakup angles  $\sim 45 - 120^\circ$ . The polarisation of the final state neutrons was determined by an ancillary large-acceptance nucleon polarimeter, surrounding a cryogenic liquid deuterium target within the Crystal Ball detector at MAMI. The polarimeter characterised  $(n, p)$  charge exchange of the ejected neutrons to determine their polarisation. The correlation of the new  $C_{x'}^n$  data with previous measurements of the induced polarisation,  $P_y^n$ , through Argand-type plots of  $C_{x'}^n - P_y^n$  are consistent with a resonant phase motion in the region of the  $d^*(2380)$  hexaquark. The new  $C_{x'}^n$  data are also compared to a theoretical model based on nucleonic and nucleon resonance degrees of freedom constrained by the current world-database of deuteron photodisintegration measurements. Structures in  $C_{x'}^n$  observed in the region of the  $d^*(2380)$  could not be explained by the purely nucleonic degrees of freedom in the model.

## 1. Introduction

Despite study for over a century [1] the photodisintegration of the deuteron, one of the most basic reactions of nuclear physics, has lacked full experimental constraint. Although the

cross section is well determined, there is a paucity of measurements of polarisation observables for the photodisintegration process. This issue is being addressed with a new programme of measurements in the A2 collaboration at MAMI to significantly expand the database of polarisation observables. The photon energies available at MAMI (0.15-1.5 GeV) enable the reaction process to be probed at distance scales where both the nucleonic and quark substructure of the deuteron play a role.

\*Corresponding author

Email address: mikhail.bashkanov@york.ac.uk (M. Bashkanov)

Such studies are of particular current importance as, alongside constraints on the role of conventional nucleon resonances and meson exchange currents, polarisation observables may provide enhanced sensitivity to more exotic QCD possibilities such as the six-quark containing (hexaquark)  $d^*(2380)$ . The  $d^*(2380)$  has recently been evidenced in a range of nucleon-nucleon scattering reactions [2, 3, 4, 5, 6, 7, 8, 9] from which quantum numbers  $I(J^P) = 0(3^+)$ , a mass  $M_{d^*} \sim 2380$  MeV and width  $\Gamma \sim 70$  MeV have been derived. In photoreactions this corresponds to a pole at  $E_\gamma \sim 570$  MeV. Constraints from photoreactions on the existence, properties and electromagnetic coupling of the  $d^*(2380)$  would have important ramifications for the emerging field of non-standard multi-quark states, and potentially for the dynamics of condensed matter systems such as neutron stars [10].

The deuteron photodisintegration reaction process [11] can be described by 12 independent complex helicity amplitudes. Achieving full information on these amplitudes requires a measurement programme of unpolarised, single-polarisation and double-polarisation observables in which combinations of photon beam polarisation, deuteron polarisation and final state nucleon polarisations are determined. We discuss the world database of measurements for deuteron photodisintegration in the relevant photon energy range, 0.15-1.5 GeV, below.

The cross section for deuteron photodisintegration in the region of the  $d^*(2380)$  has been determined over a wide range of kinematics [12](A2@MAMI). Recent measurements [13](A2@MAMI) of the single-polarisation observable  $\Sigma$ , accessed through disintegration by linearly polarised photon beams, indicated structures compatible with the mass and width of the  $d^*(2380)$  in an energy-independent polynomial analysis of the angular distributions. Measurement of the target polarisation asymmetry (T) [14](INS) also suggest anomalous structure in the  $d^*$  region, although the coarse photon energy bins achievable necessitate a future measurement with improved statistical accuracy. Measurement of the induced recoil nucleon polarisation of the final state neutron,  $P_y^n$ , has been obtained only recently, and indicated the induced neutron polarisation approaches 100% in the region of the pole of the  $d^*$  hexaquark, in a structure having width compatible with the  $d^*$  [15]. This mirrors the features observed for the induced proton polarisation [16, 17] ( $P_y^p$ ). The behaviour of both  $P_y^n$  and  $P_y^p$  cannot currently be reconciled with models including only nucleonic degrees of freedom. For double-polarisation observables, there is only a single data point in the region of the  $d^*$  from a measurement of the transferred polarisation to the ejected proton from helicity-polarised photons,  $C_{x'}^p$ , obtained at a centre-of-mass (CM) breakup angle of  $\Theta_p^{CM} \sim 90^\circ$ .

In this work, we present the first measurement (in any photon energy range) of the transferred polarisation to the neutron in deuteron photodisintegration,  $C_{x'}^n$ , which also provides the first measurement of any double-polarisation observable across the region of the  $d^*$ . The measurement was obtained using the Crystal Ball detector in A2@MAMI, sampling photon energies  $E_\gamma = 370 - 700$  MeV and CM breakup angles of  $\Theta_n^{CM} = 45 - 120^\circ$ .

The  $C_{x'}^n$  data provides new constraints on the fundamental

reaction process for deuteron photodisintegration. The data are compared to a theoretical model based on nucleon and nucleon resonance degrees of freedom in a diagrammatic approach, constrained by the current world data base of deuteron photodisintegration data. In addition a study of the (photon energy dependent) correlation between the new  $C_{x'}^n$  data and the recent  $P_y^n$  measurement [15] gives a first constraint on the existence of resonant phase motion in the region of the  $d^*$ .

## 2. Experimental Details

The measurement employed a new large acceptance neutron polarimeter [18] within the Crystal Ball detector at the A2@MAMI [19] facility during a 300 hour beamtime. A 1557 MeV longitudinally-polarised electron beam impinged on either a thin amorphous (cobalt-iron alloy) or crystalline (diamond) radiator, producing circularly (alloy) or elliptically (diamond) polarised bremsstrahlung photons. As linear photon beam polarisation is not used to extract  $C_{x'}^n$ , equal flux from the two linear polarisation settings were combined to increase the circularly-polarised yield<sup>1</sup>. The photons were energy-tagged ( $\Delta E \sim 2$  MeV) by the Glasgow-Mainz Tagger [20] and impinged on a 10 cm long liquid deuterium target cell. Reaction products were detected by the Crystal Ball (CB) [21], a highly segmented NaI(Tl) photon calorimeter covering nearly 96% of  $4\pi$  steradians. For this experiment, a new bespoke 24 element, 7 cm diameter and 30 cm long plastic-scintillator barrel (PID-POL) [22] surrounded the target, with a smaller diameter than the earlier PID detector [22], but provided similar particle identification capabilities. A 2.6 cm thick cylinder of analysing material (graphite) for nucleon polarimetry was placed around PID-POL, covering polar angles  $\Theta = 12 - 150^\circ$  and occupying the space between PID-POL and the Multi Wire Proportional Chamber (MWPC) [23]. The MWPC provided charged-particle tracking for particles passing out of the graphite into the CB. At forward angles, an additional 2.6 cm thick graphite disc covered the range  $\Theta = 2 - 12^\circ$  [22, 15]. The GEANT4 representation of the setup can be seen in Fig. 1.

The  $d(\gamma^{\circ/\otimes}, p\vec{n})$  events of interest consist of a primary ejected proton track and a kinematically reconstructed neutron, which undergoes a  $(n, p)$  charge-exchange reaction in the graphite to produce a secondary proton which subsequently produces signals in the MWPC and CB. A schematic of the experimental setup is shown in Fig. 1. The primary proton was identified using the correlation between the energy deposits in the PID and CB using  $\Delta E - E$  analysis [22] with associated track information obtained from the MWPC. The intercept of the primary proton track with the photon beamline allowed determination of the production vertex, enabling the yield originating from the target cell windows to be removed. Neutron  $^{12}\text{C}(n, p)$  charge exchange candidates required an absence of a PID-POL signal on the reconstructed neutron path into the graphite, in coincidence with a secondary proton track in the MWPC and

<sup>1</sup>The extracted  $C_{x'}^n$  for the pure circular and combined linear beam data gave consistent results within the statistical accuracy of the data.

a corresponding hit in the CB. The reconstructed incident neutron angle ( $\Theta_n$ ) was determined kinematically from  $E_\gamma$  and the production vertex coordinates. A distance of closest approach condition was imposed to ensure crossing of the (reconstructed) neutron track and the secondary proton track. Once candidate proton and neutron tracks were identified, a kinematic fit was employed to increase the sample purity and improve the determination of the reaction kinematics, exploiting the fact that the disintegration can be constrained with measurements of two kinematic quantities while three ( $\Theta_p$ ,  $T_p$  and  $\Theta_n$ ) are measured in the experiment<sup>2</sup>. A 10% cut on the probability function was used to select only events from regions where a uniform probability is observed [13].

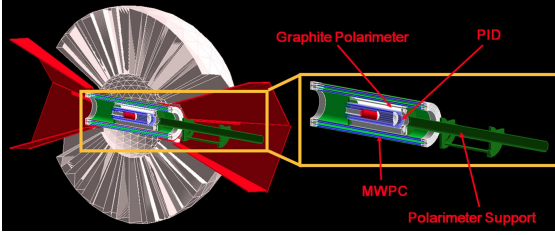


Figure 1: Crystal Ball setup during the polarimeter beamtime. The cryogenic target (red cell) is surrounded by the PID barrel (blue), the graphite polarimeter (grey), the MWPC (blue/green) and the Crystal Ball (white).

### 3. Determination of spin transfer

The transferred neutron polarisation was determined through analysis of the neutron-spin dependent  $^{12}\text{C}(n, p)$  reactions occurring in the graphite polarimeter. The spin-orbit component of the nucleon-nucleon interaction results in a azimuthal anisotropy in the produced yield of secondary protons, see Ref. [24] for details. From Ref. [26] one can define  $C_{x'}^n$  as

$$\frac{d\sigma}{d\Omega} = \left( \frac{d\sigma}{d\Omega} \right)_0 \cdot [1 + C_{x'}^n \cdot P_\gamma^\ominus \cdot P_{x'} + \dots], \quad (1)$$

where  $\left( \frac{d\sigma}{d\Omega} \right)_0$  is the unpolarised cross-section,  $C_{x'}^n$  is the spin transfer observable of interest,  $P_\gamma^\ominus$  is circular polarisation of a photon and  $P_{x'}$  is the x-projection of ejectile nucleon polarisation in the corresponding reference frame, see Fig 2. To extract the  $C_{x'}$ , one can define a likelihood function on event-by-event basis,

$$L_i = c_i \left[ 1 + C_{x'}^n \cdot P_{\gamma,i}^\ominus \cdot A_{y,i} \cdot \sin(\phi_i^{scat}) \right] A, \quad (2)$$

where  $c_i$  is a normalization coefficient,  $A$  is the detector acceptance,  $\phi_i^{scat}$  is the azimuthal angle of proton in primed frame (Fig 2) and  $A_y$  is the analysing power for the  $^{12}\text{C}(n, p)$  reaction<sup>3</sup>. A log-likelihood function was maximised to obtain the

<sup>2</sup>The fit is constrained taking the photon energy as fixed, the primary proton measured and primary neutron unmeasured.

<sup>3</sup> $P_{\gamma,i}^\ominus$  depends on photon energy only and  $A_y$  depends on ejectile neutron energy and scattered proton polar angle. Both variables are taken on event-by-event basis instead of using average values as was done in some previous analysis. Note that  $A_y$  here corresponds to the analysing power of the  $^{12}\text{C}(n, p)$  which is proportional to  $A_y(np)$  for the  $p(n, p)$  reaction.

observable of interest, given by:

$$\log L = b + \sum_i \log \left[ 1 + C_{x'}^n \cdot P_{\gamma,i}^\ominus \cdot A_{y,i} \cdot \sin(\phi_i^{scat}) \right], \quad (3)$$

where the constant  $b$  is an observable-independent constant, which absorbs the normalization coefficient and detector acceptance. The summation ( $i$ ) accounts for all events. To reduce systematic dependencies, the events were only retained if  $A_y(np) \geq 0.1$  and the proton polar scattering angle relative to the direction of the neutron  $\Theta_p^{scat} = 15 - 45^\circ$ . As  $C_{x'}^n$  is extracted as an asymmetry of yields between the two beam helicity states, acceptance and efficiency effects factor-out in the likelihood extraction. The beam helicity was flipped regularly (period of  $\sim 1$ s). Also see Ref. [15] for details of the intrinsic polarimeter acceptance and efficiency.

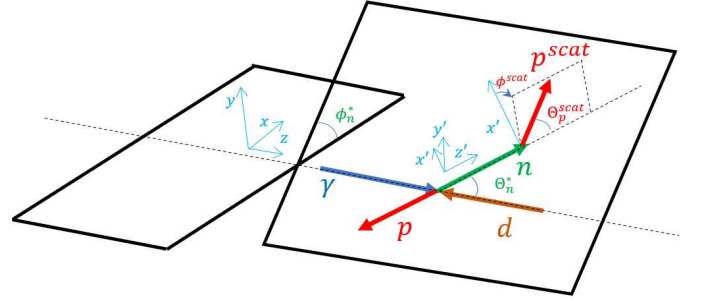


Figure 2: Kinematics of the reaction in the centre of mass system. The z-axis is oriented along the beam, y-axis is perpendicular to the ground; z' axis is oriented along the ejectile neutron direction, y' axis is perpendicular to the reaction plane.

The data were analysed using an unbinned log-likelihood analysis to minimise systematic errors produced by binned azimuthal scatter distributions. We adopt a rigorous assessment of the experimental errors in the extracted  $C_{x'}^n$  using a bootstrap procedure [25]. In this,  $C_{x'}$  is parameterised as a smooth function

$$C_{x'}^n = \sum_{i=1}^{L_{max}} a_i \cdot P_1^i(\Theta_n^*), \quad (4)$$

where  $P_1^i$  are associated Legendre functions of the first order and  $a_i$  are smooth energy dependent functions<sup>4</sup>. In our case we used  $L_{max} = 5$ . The results are largely insensitive to this choice, so long as the function covers the full parameter space (as is the case here). If  $L_{max}$  exceeds the degrees of freedom for the  $C_{x'}$  description, the decomposition coefficients would become correlated, while  $C_{x'}$  itself stays unchanged. In the bootstrap technique from our sample of  $N$  events we randomly select  $N$  events, allowing repetitions, and make a likelihood fit to extract

<sup>4</sup>In this particular case smooth functions were parameterised by equidistant (50 MeV apart) Gaussians with fixed 25 MeV  $\sigma$  and arbitrary strength. We did not force functions to be in  $[-1, 1]$  range to avoid boundary conditions artefacts, however with statistical and systematical uncertainty they all lie in this range.

$C_{x'}$  as a surface function  $C_{x'} = f(\Theta, E_\gamma)$ . Multiple repetitions of the procedure provide the most likely  $C_{x'}$  from the dataset along with its statistical and systematic errors.

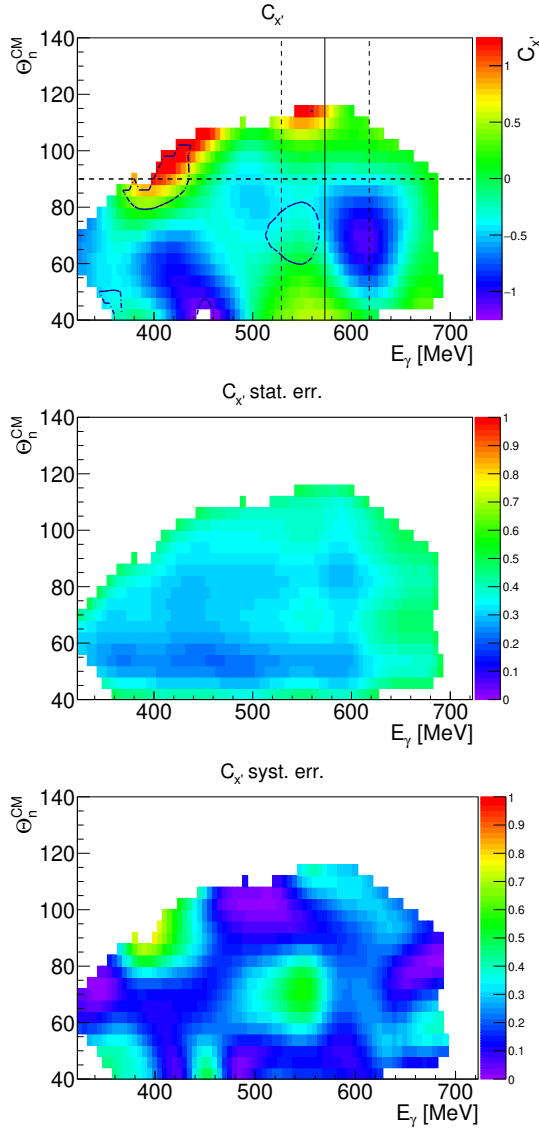


Figure 3: (Colour online) Two-dimensional  $C_{x'}^n$  dependence as a function of neutron centre-of-mass angle,  $\Theta_n^{CM}$  and photon energy,  $E_\gamma$  (top), statistical (middle) and systematic (bottom) uncertainties for this distribution. Systematic uncertainties contour lines at around 0.4 and 0.8 are also shown as on a top plot as dash-dot lines. Vertical lines show nominal  $d^*$  pole position (solid) and width (dashed).

Further studies of systematic errors in the  $C_{x'}$  extraction were obtained by relaxing the analysis cuts (increasing the minimum probability in the kinematic fit up to 40% [15]) and by comparing the outcome from the independent analysis of amorphous and diamond radiator data. The systematic errors are extracted from the resulting variations in the  $C_{x'}$ , so include significant contributions from the achievable measurement statistics. As a further check on the analysis, a parallel  $\gamma p \rightarrow n\pi^+$  analysis was performed on the same data. This reaction is well studied for this photon energy range and there is a general convergence of

the predicted  $C_{x'}$  between leading partial wave analysis groups (SAID [27] and BnGa [28, 29]). The obtained  $C_{x'}$  distributions are in statistical and systematic agreement with both SAID and BnGa predictions over the measured range of photon energies and breakup angle <sup>5</sup>.

#### 4. Results

Figure 3 (upper) shows the measured  $C_{x'}^n$  over the full sampled phase-space, along with the associated statistical (middle) and systematic (bottom) uncertainties. All the obtained  $C_{x'}^n$  data are consistent with the physical range within their statistical and systematic errors. For  $E_\gamma \sim 400 - 475$  MeV, close to the  $\Delta$  resonance, localised regions of strongly negative  $C_{x'}^n$  are observed for forward angle regions, while backwards angles of  $\sim 70^\circ - 85^\circ$  show values closer to zero. There are indications of positive  $C_{x'}^n$  at the most extreme angles, albeit associated with much larger systematic errors due to their proximity to the upper edge of the polarimeter acceptance - see Fig. 3 (bottom). The location of the pole of the  $d^*$  is shown by the solid line on Figure 3 (upper) and its width indicated by the dashed lines. Rather rapid variation of  $C_{x'}^n$  across the  $d^*$  region is observed for  $\sim \Theta_n^{CM} = 55 - 85^\circ$  - with a lobe of negative  $C_{x'}^n$  evident for photon energies above the pole and consistently smaller values below the pole. The large kinematic coverage achieved for this first determination of  $C_{x'}^n$  will clearly provide valuable new constraints on our understanding of deuteron photodisintegration.

To explore the trends in  $C_{x'}^n$  in more detail, in Fig. 4, we show  $C_{x'}^n$  (light grey line) as a function of photon energy at a fixed angle of  $\Theta_n^{CM} = 90^\circ$  (top) and  $\Theta_n^{CM} = 60^\circ$  (bottom). The statistical error bars are shown as a grey band and systematic errors as the hatched area on the bottom axis of each plot. As discussed above, the  $\Theta_n^{CM} = 90^\circ$  data suggest positive  $C_{x'}^n$  for the lower photon energies in the  $\Delta$  region below  $\sim 450$  MeV (albeit with large associated systematic errors) and negative values above this. For  $\Theta_n^{CM} = 60^\circ$ , the data indicate generally negative  $C_{x'}^n$  with a minima around 420 MeV. This arises from the "lobe" (discussed above) evident in Fig. 3 (upper). The location of this minima would therefore shift to higher photon energies for smaller  $\Theta_n^{CM}$ . Although providing first data for  $C_{x'}^n$  in the  $\Delta$  region, the current setup was not optimised for this photon energy range. Future measurements in the  $\Delta$  region with a more optimised setup i.e. higher beam polarisation (from employing a lower energy electron beam energy) and the use of thinner polarimeter material would provide data over a wider kinematic range and with smaller systematic and statistical uncertainties.

The current work focuses on regions above the  $\Delta$  to obtain the first scan of a double-polarisation observable ( $C_{x'}^n$ ) through the region of the  $d^*$ . As  $C_{x'}^n$  and the previously measured  $P_y^n$  [15] represent the real and imaginary components of the same combination of reaction amplitudes [26], then their correlation offers powerful insights. If the structure in  $P_y^n$  centred on the pole

<sup>5</sup>The results will be presented in a forthcoming publication. Note that BnGa and SAID adopt opposite sign conventions for this observable. In our work we adopt the same conventions as SAID.)

of the the  $d^*(2380)$  hexaquark [15] is indeed arising from its contribution to the imaginary part of the amplitude combination, then the real part (determined by  $C_{x'}^n$ ) should show the correlated behaviour expected from a resonance i.e. an  $s$ -shape with a central value occurring at the pole of the  $d^*(2380)$  hexaquark,  $E_\gamma \sim 570$  MeV. The photon energy dependence of  $C_{x'}^n$  does indicate such an  $s$ -shape behaviour in both angle bins. Since the  $P_y$  dependence for the  $d^*$  is expected to scale as the  $P_1^3$  associated Legendre function [15], the  $\Theta_n^{CMS} = 60^\circ$  bin is in the region of the node where  $P_y$  is expected to vanish (as  $P_1^3(\Theta = 64^\circ) = 0$ ). For such kinematics the sensitivity to the  $d^*$  in  $C_{x'}^n$  would be expected to be enhanced. It is interesting that in this angle bin the  $C_{x'}$  demonstrates an abrupt  $s$ -shape behaviour right in the region of the  $d^*$ .

For photon energies between the  $\Delta$  and the  $d^*$  region  $C_{x'}^n$  is generally negative for both angle bins. Above the  $d^*$  region, both angle bins indicate a rise in  $C_{x'}^n$  towards positive values.

The  $C_{x'}^n$  data are compared to the predictions of a theoretical model [36] based on the diagrammatic approach used earlier by other authors, see e.g. Laget [37], Levchuk [38]. The model includes photocoupling to nucleon currents, meson exchange currents and isobar (resonance) contributions from  $\Delta(1232)$ ,  $P_{11}(1440)$ ,  $D_{13}(1520)$  and  $S_{11}(1535)$  resonances. The model incorporates all available  $\gamma d \rightarrow pn$  data, including this  $C_{x'}^n$  measurement. The resulting fits are shown as the dotted curves on Fig. 4 for  $C_{x'}^n$  (blue) and  $C_{x'}^p$  (red). In the  $\Delta$  region the model is consistent with the positive  $C_{x'}^n$  data, albeit within the large systematic error of the data. However above the  $\Delta$  it is clear that this model cannot reproduce the fast varying behaviour in the region of the  $d^*$ . Such features appear inconsistent with expectations when only nucleonic and resonance degrees of freedom are included. Clearly, further theoretical calculations which include the  $d^*$  as a degree of freedom would be a critical next step - along with more detailed theoretical treatment of the resonance contributions. However, the new data provide exciting suggestions that there are features in  $C_{x'}^n$  that cannot be readily described by a model based only on nucleons and resonances and that these features are consistent with the  $d^*$  pole position and width.

It is informative to discuss the previous  $C_{x'}^p$  data (red data points in Fig. 4) and compare with the current data and theoretical models. There is a single overlapping datum at  $\Theta_p^{CM} = 90^\circ$  in this energy region. The new  $C_{x'}^n$  data indicate a comparable magnitude to this single  $C_{x'}^p$  datum at  $E_\gamma = 475$  MeV. Two  $C_{x'}^p$  data points at higher photon energies than the current data are also shown. The Fix model [36] (red dotted line) gives a good description of the single  $C_{x'}^p$  datum. Two previous models for deuteron photodisintegration gave predictions for  $C_{x'}^p$ . The coupled channel calculation of  $C_{x'}^p$  from Arenhoevel [31] (black solid line; adopted from [26]) has a more limited photon energy range due to only low lying resonances being included. This model shows good agreement with the (subsequently obtained)  $C_{x'}^p$  datum although giving different predictions to the Fix model in the  $\Delta$  region. The relativistic model of Kang [30] (black dashed line) predicts an opposite sign for  $C_{x'}^p$  than evidenced in the data. Both the Arenhoevel and Kang predictions exhibit a smooth variation in  $C_{x'}^p$  in the region of the  $d^*$ , lacking

the  $s$ -shape features indicated in the  $C_{x'}^n$  data (this is naively to be expected for such nucleonic based models as there are no nucleon resonances entering the disintegration mechanism in this region). Above 700 MeV, Kang predicts a negative  $C_{x'}^n$ , with an  $s$ -shape behaviour, attributable to the  $N^*(1520)$  resonance with a central value at 760 MeV. However, in this region, the sign of the Kang predictions are in disagreement with the  $C_{x'}^p$  data. Unfortunately, both these calculations were only published at this single breakup angle so no comparison for the  $\Theta_p^{CM} = 60^\circ$  bin can be made.

Since  $C_{x'}$  and  $P_y$  are real and imaginary parts of the same combination of amplitudes [26], and since these amplitudes indicate sensitivity to the  $d^*(2380)$ , an Argand-type plot allows more detailed study of any phase motion from a resonance contribution. The two observables  $C_{x'}$  and  $P_y$  are plotted in a 2D Argand-type plot in Fig. 5. Data from all photon energies are plotted as a locus. The photon energy at various points on the locus are arbitrarily labelled by the red data points (note the analysis uses an unbinned method so these are to guide the eye and do not correspond to actual bins). There is some indication of looping on the Argand plot, as expected from a resonance contribution, between 500-600 MeV. We should remark that for a resonance in the presence of backgrounds and interference some distortion would be expected compared to a pure resonance. The diameter of a resonance loop on an Argand diagram is directly related to the branching ratio of the resonance to the channel under study. For resonances with small branching ratios, small radius loops are expected. The  $d^*(2380)$  branch into  $pn$  is large ( $\sim 12\%$  [32]), but the  $\gamma d \rightarrow d^*$  branch is small ( $\sim 10^{-3}\%$  [33, 34]) leading to an expectation of structures with small radii from a  $d^*$  contribution. Also shown on the figure (dashed blue curve) are the theoretical predictions of Fix [36] for nucleonic, resonance and MEC mechanisms. It is clear the model does not reproduce the tight looping of the data, or the large  $P_y$  values in the region of the  $d^*$ .

## 5. Summary

The neutron spin-transfer coefficient  $C_{x'}^n$  in deuteron photodisintegration has been measured for  $E_\gamma = 370 - 700$  MeV and photon-deuteron centre-of-mass breakup angles for the proton of  $40 - 120^\circ$ , providing the first measurement of this fundamental observable. The data are at variance with all existing theoretical models based on purely nucleon resonance contributions. A narrow  $s$ -shape structure centred around  $E_\gamma \sim 570$  MeV is observed and is complementary to the ‘‘anomalous’’ structure observed previously for the recoil proton and neutron polarisations  $P_y^{p,n}$  [16, 15]. In a simple ansatz, the photon energy and angular dependencies of this ‘‘anomaly’’ are consistent with a contribution from the  $J^P = 3^+ d^*(2380)$  hexaquark. The photon energy dependent correlation between the new  $C_{x'}^n$  data and previous  $P_y^N$  measurements suggests a looping behaviour consistent with the expected role of a  $d^*$  resonance.

The new  $C_{x'}^n$  data will be combined with future measurements of polarisation observables in deuteron photodisintegration with a polarised photon beam and transversely polarised

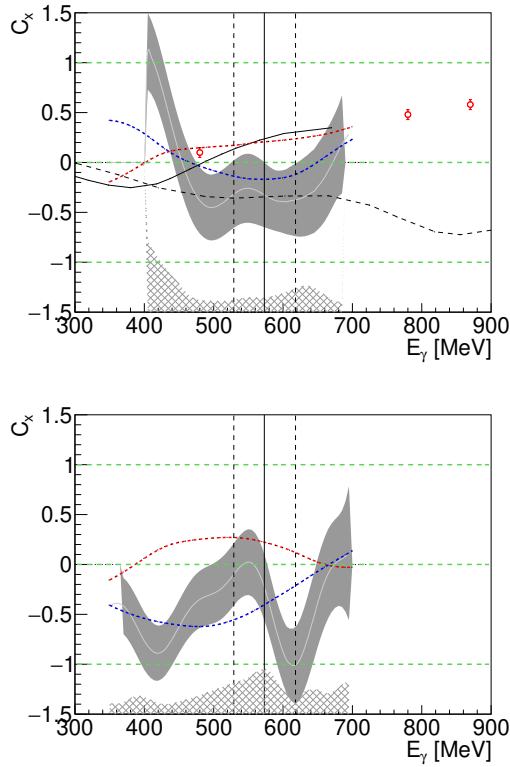


Figure 4:  $C_x^n$  for the  $\Theta_n^{CMS} = 90^\circ$  (top) and  $\Theta_n^{CMS} = 60^\circ$  (bottom) are shown as a light grey line with statistical errors as a grey band and systematic errors as the hatched area on the bottom axis of each plot. Previous  $C_x^n$  from Ref. [35] are shown as red squares. Calculations for  $C_x^n$  from Ref. [31] (Arenhoevel) and Ref. [30] (Kang) are shown as solid and dashed black lines respectively. Calculations for  $C_x^n$  (red) and  $C_x^n$  (blue) from Ref. [36] (Fix) are shown as dotted lines. Vertical lines show nominal  $d^*$  pole position (solid) and width (dashed).

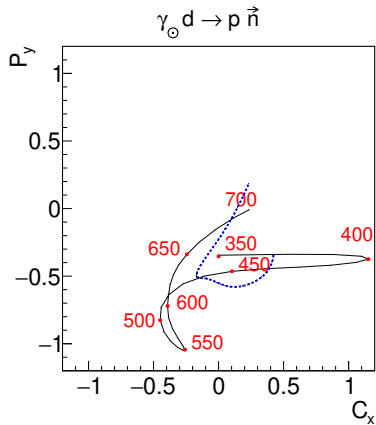


Figure 5: An Argand-style plot of  $C_x^n$  from this work vs  $P_y^n$  from Ref. [15] at  $\Theta_n^{CMS} = 90^\circ$ . Calculations from Ref. [36](A.Fix) for the same quantity is shown as a dotted blue line.

deuteron target at MAMI, progressing towards a first well-constrained partial wave analysis of the fundamental deuteron photodisintegration reaction.

## 6. Acknowledgements

We are indebted to M. Zurek for providing us data on  $n^{12}\text{C}$  analysing powers. All data are available for downloading from PURE [39]. This work has been supported by the U.K. STFC (ST/V002570/1, ST/L00478X/2, ST/V001035/1, ST/P004385/2, ST/T002077/1, ST/L005824/1, 57071/1, 50727/1 ) grants, the Deutsche Forschungsgemeinschaft (SFB443, SFB/TR16, and SFB1044), DFG-RFBR (Grant No. 09-02-91330), Schweizerischer Nationalfonds (Contracts No. 200020-175807, No. 200020-156983, No. 132799, No. 121781, No. 117601), the U.S. Department of Energy (Offices of Science and Nuclear Physics, Awards No. DE-SC0014323, DEFG02-99-ER41110, No. DE-FG02-88ER40415, No. DEFG02-01-ER41194) and National Science Foundation (Grants NSF OISE-1358175; PHY-1039130, PHY-1714833, No. IIA-1358175), INFN (Italy), and NSERC of Canada (Grant No. FRN-SAPPJ2015-00023).

## References

- [1] J. Chadwick, M. Goldhaber, *Nature* **134**, 237, (1934).
- [2] M. Bashkanov *et al.*, *Phys. Rev. Lett.* **102**, 052301, (2009).
- [3] P. Adlarson *et al.*, *Phys. Rev. Lett.* **106**, 242302, (2011).
- [4] P. Adlarson *et al.*, *Phys. Lett. B* **721**, 229, (2013).
- [5] P. Adlarson *et al.*, *Phys. Rev. C* **88**, 055208, (2013).
- [6] P. Adlarson *et al.*, *Phys. Lett. B* **743**, 325, (2015).
- [7] P. Adlarson *et al.*, *Eur. Phys. J. A* **52**, 147, (2016).
- [8] P. Adlarson *et al.*, *Phys. Rev. Lett.* **112**, 202301, (2014).
- [9] P. Adlarson *et al.*, *Phys. Rev. C* **90**, 035204, (2014).
- [10] I. Vidaña, M. Bashkanov, D.P. Watts, A. Pastore, *Phys. Lett. B* **781**, 112-116, (2018).
- [11] H. Arenhövel and M. Sanzone "Photodisintegration of the Deuteron: A Review of Theory and Experiment", Springer Verlag, (1991).
- [12] R. Crawford *et al.*, *Nucl. Phys. A* **603**, 303, (1996).
- [13] M. Bashkanov *et al.*, *Phys. Lett. B* **789**, 7, (2019).
- [14] Y. Ohashi *et al.*, *Phys. Rev. C* **36**, 2422, (1987).
- [15] M. Bashkanov *et al.*, *Phys. Rev. Lett.* **124**, 132001, (2020).
- [16] H. Ikeda *et al.*, *Phys. Rev. Lett.* **42**, 1321, (1979).
- [17] T. Kamae, T. Fujita, *Phys. Rev. Lett.* **38**, 471, (1977).
- [18] D.P. Watts, J.R.M Annand, M. Bashkanov, D.I Glazier, MAMI Proposal Nr. A2/03-09, [http://bamboo.pv.infn.it/Mambo/MAMI/prop\\_2009/MAMI-A2-03-09.pdf](http://bamboo.pv.infn.it/Mambo/MAMI/prop_2009/MAMI-A2-03-09.pdf)
- [19] K.-H. Kaiser *et al.*, *Nucl. Instr. Meth. A* **593**, 159, (2008).
- [20] J.C. McGeorge *et al.*, *Eur. Phys. J. A* **37**, 129, (2008).
- [21] A. Starostin *et al.*, *Phys. Rev. C* **64**, 055205, (2001).
- [22] S.J.D. Kay, Ph.D. thesis, University of Edinburgh, 2018, <https://www.era.lib.ed.ac.uk/handle/1842/31525>.
- [23] G. Audit *et al.*, *Nucl. Instr. Meth. A* **301**, 473, (1991).
- [24] SAID data base <http://gwdac.phys.gwu.edu/>; R. A. Arndt *et al.*, *Phys. Rev. C* **76**, 025209, (2007).
- [25] A. Pastore, *J. Phys. G*, **46**, 052001, (2019).
- [26] R. Gilman, F. Gross, *J. Phys. G* **28**, R37, (2002).
- [27] W. J. Briscoe *et al.*, *Phys. Rev. C* **100**, 065205, (2019).
- [28] N. Zachariou *et al.*, *Phys. Lett. B* **817**, 136304, (2021).
- [29] A.V. Anisovich *et al.*, *Eur.Phys.J. A* **52**, 284, (2016).
- [30] Y. Kang, (1993), Ph.D. thesis Bonn.
- [31] M. Schwamb and H. Arenhövel, *Nucl. Phys. A* **690**, 647 and 682, (2001).
- [32] M. Bashkanov, H. Clement, T. Skorodko, *Eur. Phys. J. A* **51**, 7, 87, (2015).
- [33] T. Ishikawa *et al.*, *Phys. Lett. B* **789**, 413, (2019).
- [34] T. Jude *et al.*, *nucl-ex: 2202.08594*.
- [35] K. Wijesooriya *et al.*, *Phys. Rev. Lett.*, **86**, 2975, (2001).
- [36] A. Fix, private communications.
- [37] R. Crawford *et al.*, *Nucl. Phys. A* **603**, 303, (1996).
- [38] M. I. Levchuk, *Few Body Syst.* **19**, 77-108, (1995)
- [39] <https://pure.york.ac.uk/>.